Numerical study of unsteady mixed convection stagnation point flow over a stretching cylinder with sinusoidal surface temperature

A. Majeed[a,*], T. Javed[a], A. Ghaffari[a], and I. Pop[b]
[a]*Department of Mathematics and Statistics, FBAS, International Islamic University, Islamabad 44000, Pakistan.*
[b]*Faculty of Mathematics, and Statistics, University of Cluj, R-3400 Cluj, CP 253, Romania.*
[*]*Tel.: +923335251806; e-mail: abidmajeed726@yahoo.com*

Received 8 December 2015; accepted 4 February 2016

The paper provides the analysis of unsteady two-dimensional mixed convection stagnation point flow over a vertical stretching cylinder with sinusoidal wall temperature. The governing partial differential equations are converted into dimensionless form by using suitable transformations. For the numerical solution of dimensionless partial differential equations, an implicit finite difference scheme namely Keller Box method is applied. The comparison is made to show the accuracy of our results with literature for some special cases. Graphs of velocity and temperature profiles are plotted for assisting and opposing flow cases at fixed value of time. The assisting buoyant flow augment the momentum boundary layer while opposing buoyant flow show opposite behavior. The thermal boundary layer thickness grows with the passage of time. Skin friction and Nusselt number are plotted for unsteadiness parameter and amplitude of surface temperature oscillations against time. It is apparent that as the values of surface temperature oscillations drops, the amplitude of oscillations in skin friction and Nusselt number also drops. Furthermore, isotherms are drawn to exhibit the influence of the amplitude of oscillations on curvature parameter with time.

Keywords: Stretching cylinder; boundary layer flow; mixed convection; finite difference method; sinusoidal wall temperature.

PACS: 47.15.cb; 47.10.ad; 47.11.Bc

1. Introduction

The stagnation point encounters highest pressure, enhancement of heat transfer and rate of mass deposition. Some practical examples are cooling of electronic devices by fans, cooling of nuclear reactors during emergency shutdown, heat exchangers placed in a low velocity environment, solar central receivers exposed to wind current and many others [1]. Due to these aspects, the study of stagnation point flow and heat transfer has attracted many researchers and engineers. Hiemenz [2] initiated the study of two dimensional stagnation point flow over a stationary flat plate. He transformed the Navier-Stokes equations into ordinary differential equations by using similarity transformations and provided the exact solution of the nonlinear differential equations. Homann [3] extended this work to three dimensional problem of axisymmetric stagnation-point flow. Schlichting and Bussmann [4] provided numerical solution of Hiemenz problem and Eckert [5] also extended the work of Heimenz [2] by incorporating heat transfer rate in the stagnation point flow. Ariel [6] obtained the analytical solution by introducing suction in flow field. Stagnation point flow over moving surfaces is also significant in practical purposes including paper production, the spinning of fibres, glass blowing, continuous metal casting [7], manufacturing of sheeting material through extrusion process especially in the polymer extrusion in a melt spinning process, aerodynamic extrusion of plastic sheets [8] etc. Chiam [9] investigated two-dimensional stagnation point flow of a viscous fluid over a linear stretching surface. He considered the situation where stretching velocity is equal to straining (free stream) velocity and concluded that no boundary layer exist in this case. Contrary to the Chiam [9], Mahapatra and Gupta in [10,11], analysed the effects of magnetohydrodynamics and heat transfer respectively, in the region of stagnation point flow towards a stretching surface. They showed that the boundary layer is formed when $a/c > 1$ (ratio of straining to stretching velocity) and inverted boundary layer is emerge when $a/c < 1$. Unsteady analysis of flow over a stretching sheet is reported by Nazar *et al*., [12]. Recently, Mustafa *et al*. [13], Bhattacharyya *et al*., [14], Sharma and Singh [15], Bhattacharyya *et al*., [16], and Javed *et al*., [17] reported the investigations on the stagnation point flow over linear and non-linear stretching/shrinking sheets in different aspects. Wang [18] did the pioneering work and investigated the fluid flow due to stretching cylinder. Ishak *et al*. [19,20] extended the work of Wang [18] by including the heat transfer effects due to impermeable stretching cylinder by considering suction and injection cases. They produced numerical and perturbation solutions of the flow problem. Inspired by previous work, many researchers performed their analysis over stretching cylinder with Newtonian and non-Newtonian fluids [21-27] and incorporating innumerable physical configurations. In all aforementioned studies, the investigations carried out with temporally constant surface condition and the transient development of flow and heat transfer over stretching cylinder is not extensively studied. Merkin [28] stated that the value of surface temperature does not remains constant, it often fluctuate about some mean value. The influence of time dependent oscillations in surface conditions has received very little attention to date.

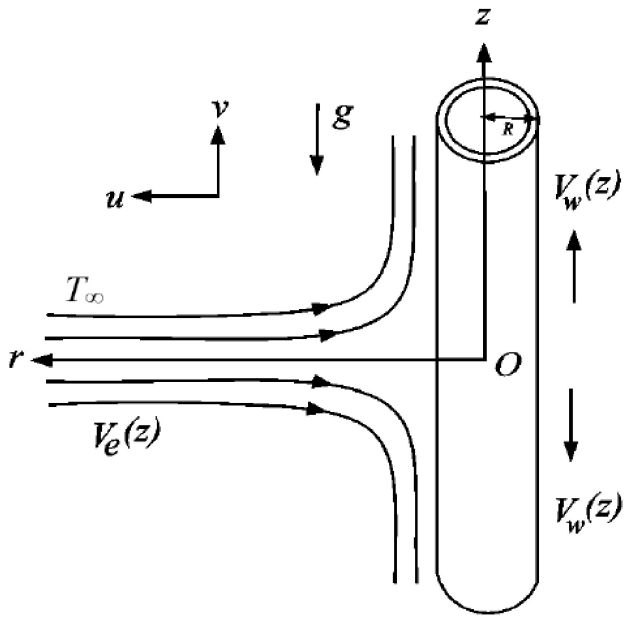

FIGURE 1. Physical Model of the problem.

The aim of this paper is to study the unsteady mixed convection stagnation point flow over a cylinder with sinusoidal time dependent wall temperature. Graphs for velocity and temperature profiles, skin friction coefficient, Nusselt number and isotherms are plotted for various governing parameters.

2. Problem formulation

We consider two dimensional unsteady laminar boundary layer fluid flow near the stagnation point over a cylinder as shown in Fig. 1. The cylinder is of radius r is permeable and continuously stretching with velocity $V_w(z)$ along its own axis. To investigate the analysis, a cylindrical coordinate system is considered as such that the *z*-axis is taken along the axis of the cylinder and the *r*-axis is in the radial direction. It is assumed that the stretching (V_w) and straining (V_e) velocities are proportional to distance *z* from the stagnation point *i.e.*, $V_w = cz/l$ and $V_e = az/l$. The temperature at the surface of cylinder (T_w) is considered to be sinusoidal and the ambient fluid temperature is T_∞ such that ($T_w > T_\infty$). The unsteady boundary layer equations with Boussinesq approximation and viscous dissipation for continuity, momentum and energy equations are given by

$$\frac{\partial(rv)}{\partial z} + \frac{\partial(ru)}{\partial r} = 0, \tag{1}$$

$$\frac{\partial v}{\partial t} + u\frac{\partial v}{\partial r} + v\frac{\partial v}{\partial z} = V_e\frac{\partial V_e}{\partial z} + \nu\left(\frac{\partial^2 v}{\partial v^2} + \frac{1}{r}\frac{\partial v}{\partial r}\right) + g\beta_t(T - T_\infty), \tag{2}$$

$$\frac{\partial T}{\partial t} + u\frac{\partial T}{\partial r} + v\frac{\partial T}{\partial z} = \alpha\left(\frac{\partial^2 T}{\partial r^2} + \frac{1}{r}\frac{\partial T}{\partial r}\right). \tag{3}$$

The boundary conditions of the assumed flow are

$$\begin{aligned} v = V_w = \frac{cz}{l}, \quad u = U_0, \\ T = T_w(z) = T_\infty \\ + T_0\Big(\frac{z}{l}\Big)(1 + \varepsilon\sin\omega t) \quad \text{at} \quad r = R, \\ v \to V_e = \frac{az}{l}, \quad T \to T_\infty \quad \text{as} \quad r \to \infty. \end{aligned} \tag{4}$$

where *u* and *v* are the velocity components along *r* and *z* directions, respectively, *T* is the temperature of the fluid within the boundary layer, ν is the kinematic viscosity, *g* is the acceleration due to gravity, β_t is the thermal expansion coefficient, α is the thermal diffusivity, μ is the dynamic viscosity of fluid, ρ is the fluid density, c_p is the specific heat constant, U_0 is the mass flux velocity, T_0 is some temperature scale, *t* is the time, ϵ is the amplitude of surface temperature oscillation and ω is the frequency of the oscillation. Introducing the following non-dimensional variables

$$\begin{aligned} \eta = \frac{r^2 - R^2}{2R}\sqrt{\frac{c}{\nu l}}, \psi = \sqrt{\frac{\nu c}{l}}zRf(\eta,\tau),\tau \\ = \omega t, T = T_\infty + T_0\Big(\frac{z}{l}\Big)\theta(\eta,\tau) \end{aligned} \tag{5}$$

In which, η is the similarity variable, ψ is the stream function defined as $u = r^{-1}\partial\psi/\partial r$ and $v = -r^{-1}\partial\psi/\partial z$ which identically satisfies Eq. (1), $f(\eta,\tau)$ is the dimensionless function and $\theta(\eta,\tau)$ is the dimensionless temperature field. From relation (5), we obtain

$$u = -\frac{R}{r}\sqrt{\frac{\nu c}{l}}f(\eta,\tau), \quad \text{and} \quad v = \frac{cz}{l}f_\eta(\eta,\tau) \tag{6}$$

Substituting Eqs. (5) and (6) into Eqs. (2) and (3), we get the following dimensionless system of partial differential equations

$$(1 + 2\gamma\eta)f_{\eta\eta\eta} + 2\gamma f_{\eta\eta} + ff_{\eta\eta} + \Big(\frac{a}{c}\Big)^2 - f_\eta^2 + \lambda\theta - \beta f_{\eta\tau} = 0 \tag{7}$$

$$(1 + 2\gamma\eta)\theta_{\eta\eta} + 2\gamma\theta_\eta + Pr(f\theta_\eta - f_\eta\theta - \beta\theta_\tau) = 0 \tag{8}$$

The boundary conditions in Eq. (4) become

$$\begin{aligned} \eta = 0: \quad f(\eta,\tau) = S, \\ f_\eta(\eta,\tau) = 1, \quad \theta(\eta,\tau) = 1 + \epsilon\sin\tau, \end{aligned} \tag{9}$$

$$\eta \to \infty: \quad \theta(\eta,\tau) = 0, \quad f_\eta(\eta,\tau) = \frac{a}{c}, \tag{10}$$

where $\gamma = \sqrt{\nu l/cR^2}$ is curvature parameter, a/c is the ratio of straining (free stream) to stretching velocities, $\lambda = Gr_z/Re_z^2$ is the mixed convection parameter ($Gr_z = g\beta_t T_0 z^4/l\nu^2$) and ($Re_z = cz^2/l\nu$). It is important to note that $\lambda = 0$ corresponds to forced convection flow, $\lambda > 0$ ($T_0 > 0$) corresponds to assisting flow (*i.e.*, the

buoyancy forces acts parallel to free stream velocity), $\lambda < 0$ ($T_0 < 0$) corresponds to opposing flow (*i.e.*, the buoyancy forces acts opposite to free stream velocity), $\beta = l\omega/c$ is unsteady parameter (arises due to temperature oscillations), Pr$= \nu/\alpha$ is Prandtl number, *S* is the suction/injection parameter with $S > 0$ represents suction case and $S < 0$ is for injection case. The quantities of physical interest are the skin friction coefficient C_f and the local Nusselt number Nu_z which are defined as:

$$C_f = \frac{\tau_w}{\rho V_w^2}, \qquad Nu_z = \frac{q_w l}{kT_0} \tag{11}$$

in which the wall skin friction (τ_w) and the wall heat flux (q_w) are

$$\tau_w = \mu \left(\frac{\partial v}{\partial r}\right)_{r=R}, \qquad q_w = -k \left(\frac{\partial T}{\partial r}\right)_{r=R} \tag{12}$$

Using the transformation (5) the skin friction coefficient and the local Nusselt number can be written as

$$Re_z^{1/2} C_f = f_{\eta\eta}(0,\tau), \quad Re_z^{-1/2} Nu_z = -\theta_\eta(0,\tau). \tag{13}$$

3. Numerical solution procedure

The nonlinear partial differential Eqs. (7) and (8) subject to the boundary conditions (9) are solved by using an implicit finite difference second order accurate scheme known as Keller Box method. The detailed method has explained in the book by Cebeci and Bradshaw [29]. The main steps are follows:

Step I: Eqs. (8) and (9) are reduced into first order differential after letting

$$f_\eta = U, \qquad U_\eta = V, \qquad \theta_\eta = Q$$

as follows

$$(1+2\gamma\eta)V_\eta + 2\gamma V + fV + (a/c)^2 + U^2 + \lambda\theta - \beta U_\tau = 0,$$
$$(1+2\gamma\eta)Q_\eta + 2\gamma Q + Pr(fQ - U\theta - \beta\theta_\tau) = 0,$$

with boundary conditions

$$f(0,\tau) = S, \quad U(0,\tau) = 1,$$
$$\theta(0,\tau) = 1 + \epsilon \sin\tau, \quad \theta(\infty,\tau) = 0, \quad U(\infty,\tau) = a/c$$

Step II: The derivatives in η and τ-direction are replaced by central differences at $j - 1/2$ and $n - 1/2$ positions respectively as follows

$$(\quad)^n_{j-1/2} = \frac{1}{h}\left((\quad)^n_j - (\quad)^n_{j-1}\right),$$
$$(\quad)^{n-1/2}_j = \frac{1}{k}\left((\quad)^n_j - (\quad)^{n-1}_j\right).$$

TABLE I. Numerical values of $f_{\eta\eta}(0,\tau)$ for various values of a/c when $\gamma = \lambda = S = \beta = \tau = 0$ with Mahapatra and Gupta [11] and Nazar *et al*. [12].

a/c	Ref. 11	Ref. 12	Present study
0.01		-0.998	-0.998
0.02		-0.9958	-0.9958
0.05		-0.9876	-0.9876
0.1	-0.9694	-0.9694	-0.9694
0.2	-0.9181	-0.9181	-0.9181
0.5	-0.6673	-0.6673	-0.6673
2	2.0175	2.0176	2.0175
3	4.7293	4.7296	4.7294
5		11.7537	11.7524
10		36.2687	36.2603
20		106.5744	106.5239
50		430.6647	430.1501

However, the values of the functions are replaced by its mean value like

$$(\quad)^n_{j-1/2} = \frac{1}{2}\left((\quad)^n_j + (\quad)^n_{j-1}\right),$$
$$(\quad)^{n-1/2}_j = \frac{1}{2}\left((\quad)^n_j + (\quad)^{n-1}_j\right).$$

and as a result, the nonlinear system of algebraic equations is obtained.

Step III: To handle the non-linearity of resulting system of algebraic equations, Newton's linearization process is implemented. For $(i+1)^{th}$ iterations, we write for every unknown function $f_j^{i+1} = f_j^i + \delta f_j^i$, we obtained the system of linear equations.

Step IV: The obtained system of linear equations is solved by block tri-diagonal technique. The edge of boundary layer thickness η_∞ is chosen according to the values of the parameters. The iteration is continued for refinement in the solution until we achieved the difference between two consecutive iterations is less than 10^6. The employed technique is validated after comparing the numerical values of $f_{\eta\eta}(0,\tau)$ with Mahapatra and Gupta [11] and Nazar *et al*. [12] as shown in Table I as a limiting case. Table II gives the comparison of $-\theta_\eta(0,\tau)$ with Ishak *et al*. [28] for limited cases. These results are in good agreement that gives us a confidence in accuracy of the employed numerical technique.

4. Results and Discussion

The non-linear partial differential Eqs. (7-8) subject to the boundary conditions (9) are solved numerically using very efficient implicit scheme known as Keller Box method for

TABLE II. Comparsion of $-\theta_\eta(0,\tau)$ for various values of λ and Pr when $\gamma = a/c = S = \beta = \epsilon = 0$ with Ishak *et al.* [29].

λ	Pr	Ref. 29	Present study
0	0.01	0.0197	0.0198
	0.72	0.8086	0.8086
	1	1	1
	3	1.9237	1.9237
	7	3.0723	3.0723
	10	3.7207	3.7208
	100	12.2941	12.3004
1	1	1.0873	1.0873
2		1.1423	1.1423
3		1.1853	1.1853

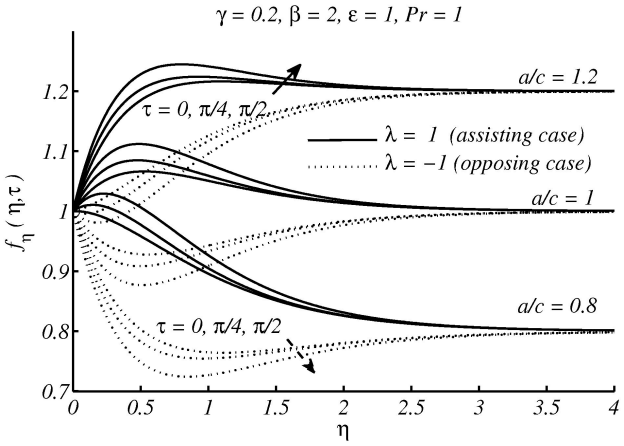

FIGURE 2. Velocity profile for $\lambda = 1$ (assisting flow) and $\lambda = -1$ (opposing flow).

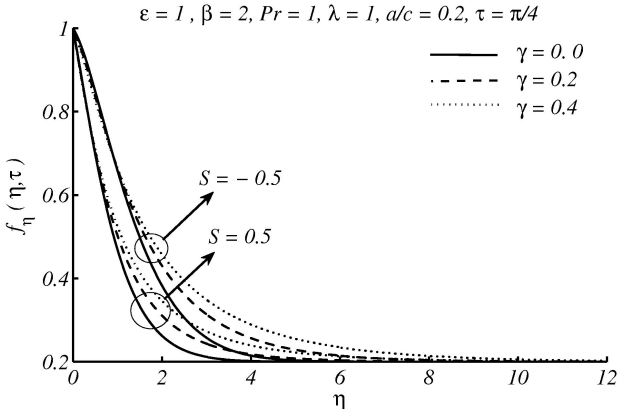

FIGURE 3. Velocity profile for different values of γ at $S = 0.5$ (suction) and $S = -0.5$ (injection).

various values of emerging dimensionless parameters namely, curvature parameter (γ), velocity ratio parameter (a/c), mixed convection parameter (λ), suction/injection parameter (S), unsteadiness parameter (β), Prandtl number (Pr)

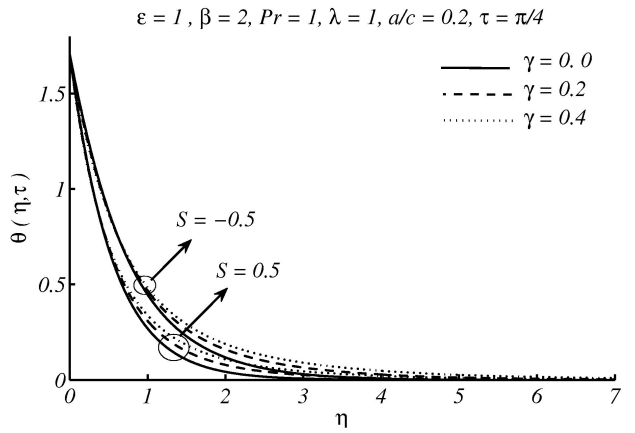

FIGURE 4. Temperature profile for various values of γ at $S = 0.5$ (suction) and $S = -0.5$ (injection).

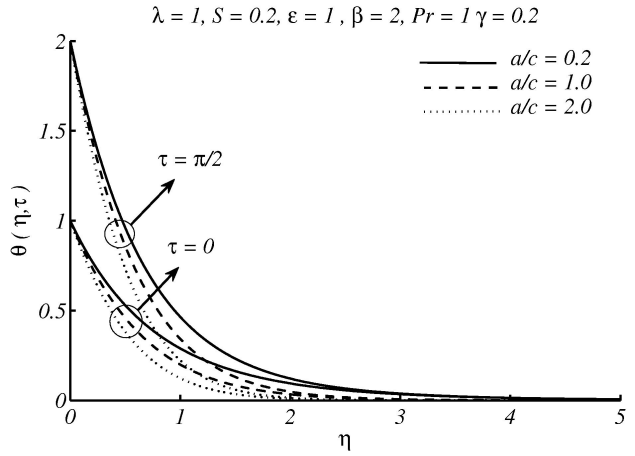

FIGURE 5. Temperature profile for various value of a/c at time $\tau = 0$ and $\tau = \pi/2$.

and amplitude of oscillation in temperature (ϵ). The numerical results are computed in terms of velocity and temperature profiles, skin friction coefficient and Nusselt number. Figure 2 exhibits the velocity profile for different values of a/c for assisting case ($\lambda = 1$) and opposing case ($\lambda = 1$) at different time steps levels ($\tau = 0, \pi/4, \pi/2$). It is observed that velocity increases for increasing values of time (τ) in assisting flow case ($\lambda = 1$) and opposite behavior is observed in opposing flow case ($\lambda = -1$). This is due to the reason that in assisting flow, buoyant force assist the flow and in opposing flow, buoyant force delays the flow. Figures 3 and 4 show the velocity and temperature profiles for various values of curvature parameter (γ) and suction/injection parameter (S). In Fig. 3, it is noted that the velocity profile decreases near the surface of cylinder and increases far away from the surface with increase in curvature parameter (γ) for both suction ($S = 0.5$) and injection ($S = -0.5$) parameter. It is also observed that in case of injection ($S = -0.5$), the velocity and momentum boundary layer thickness become higher as compare to suction ($S = 0.5$). This is because injection enhances the flow near the surface. In Fig. 4 for both values of suction/injection parameter (S), the temperature profile in-

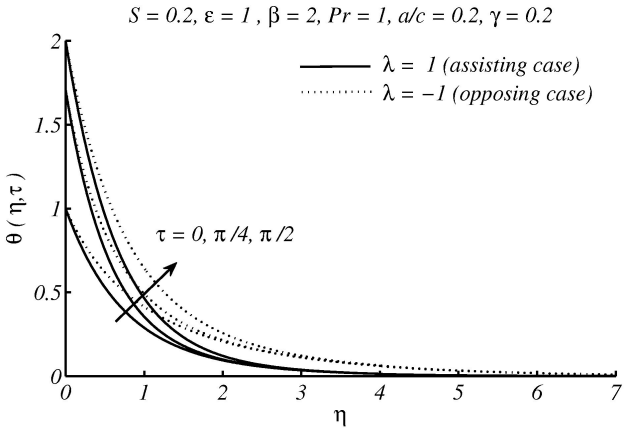

FIGURE 6. Temperature profile for various values of τ.

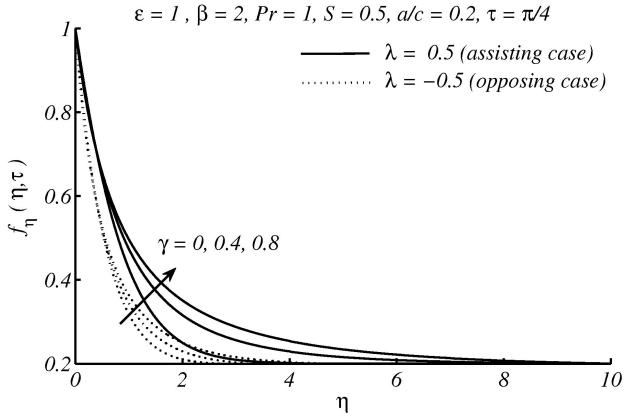

FIGURE 7. Velocity profile for various values of γ.

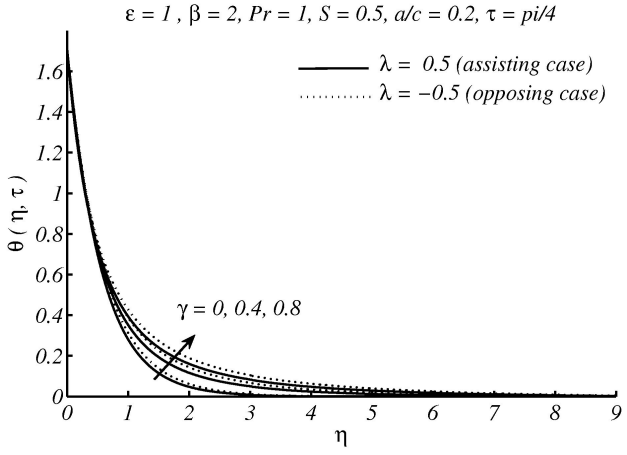

FIGURE 8. Temperature profile for various values of γ.

creases with increase in curvature of the cylinder. It is further noted that, thermal boundary layer thickness can be increased with increase in curvature parameter (γ) both for injection/suction cases. Figure 5 demonstrates the effects on temperature profiles for various values of velocity ratio parameter (a/c) at different time step levels $\tau = 0$ and $\pi/2$. The temperature profile increase with the increasing value of

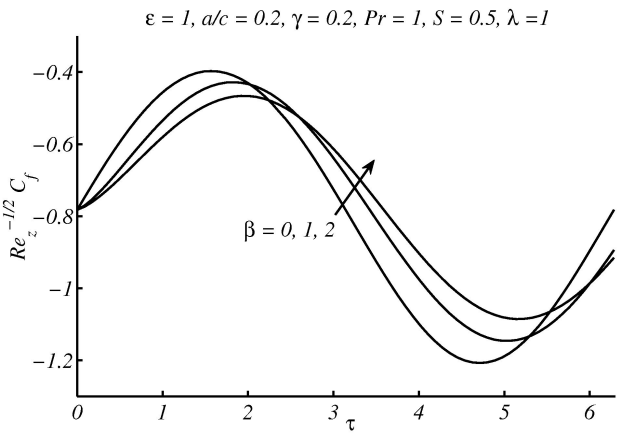

FIGURE 9. Variation of skin friction coefficient against time for different values of β.

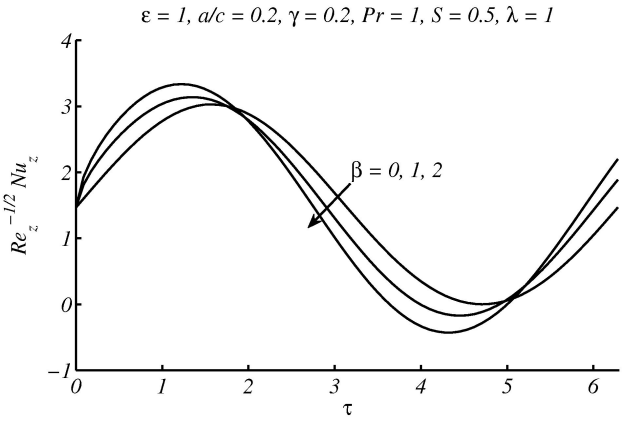

FIGURE 10. Variation of local Nusselt number against time for different values of β.

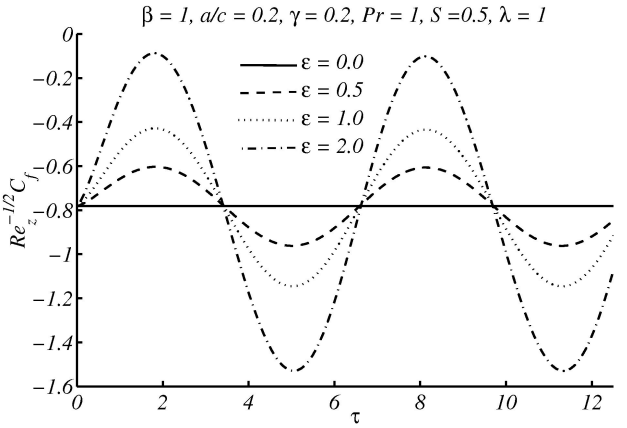

FIGURE 11. Variation of skin friction coefficient against time for different values of ϵ.

time (τ) for all values of a/c. It is further important to note that the temperature profile decreases due to velocity ratio parameter (a/c) and hence thermal boundary layer thickness become smaller for large values of velocity ratio parameter (a/c). In Fig. 6, the temperature profile increases within the boundary layer for increasing time steps levels in both as-

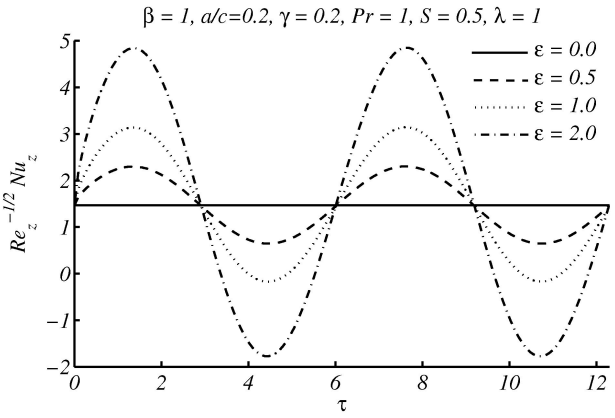

FIGURE 12. Variation of local Nusselt number against time for different values of ϵ.

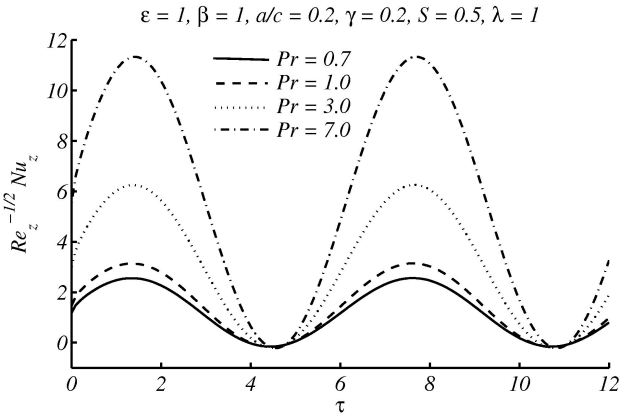

FIGURE 13. Variation of local Nusselt number against time for different values of Pr.

sisting and opposing flow cases. In opposing flow case the thermal boundary layer thickness is larger as compared to assisting flow case for all time steps levels ($\tau = 0, \pi/4, \pi/2$). Influence of curvature parameter (γ) on velocity and temperature profile for (assisting flow) and (opposing flow) is shown in Figs. 7 and 8, respectively. As curvature parameter (γ) increases the surface of cylinder squeezes due to which surface area reduces. As a result velocity of the fluid increases with increase in curvature parameter (γ). Similarly temperature of the fluid also enhances within the boundary layer region due to increase in curvature parameter (γ). In addition, momentum boundary layer augments in case of $\lambda = 0.5$(assisting flow) in comparison with $\lambda = -0.5$(opposing flow) but very little change is observed in momentum boundary layer for $\lambda = 0.5$ (assisting flow) and $\lambda = -0.5$(opposing flow) cases. Figures 9 and 10 illustrate the variations in skin friction coefficient and Nusselt number against time (τ) for different values of unsteadiness parameter (β). Due to sinusoidal nature of temperature, the amplitude of skin friction enhanced with backward phase shift against time (τ) with increase in unsteadiness parameter (β). Figures 11 and 12 show the val-

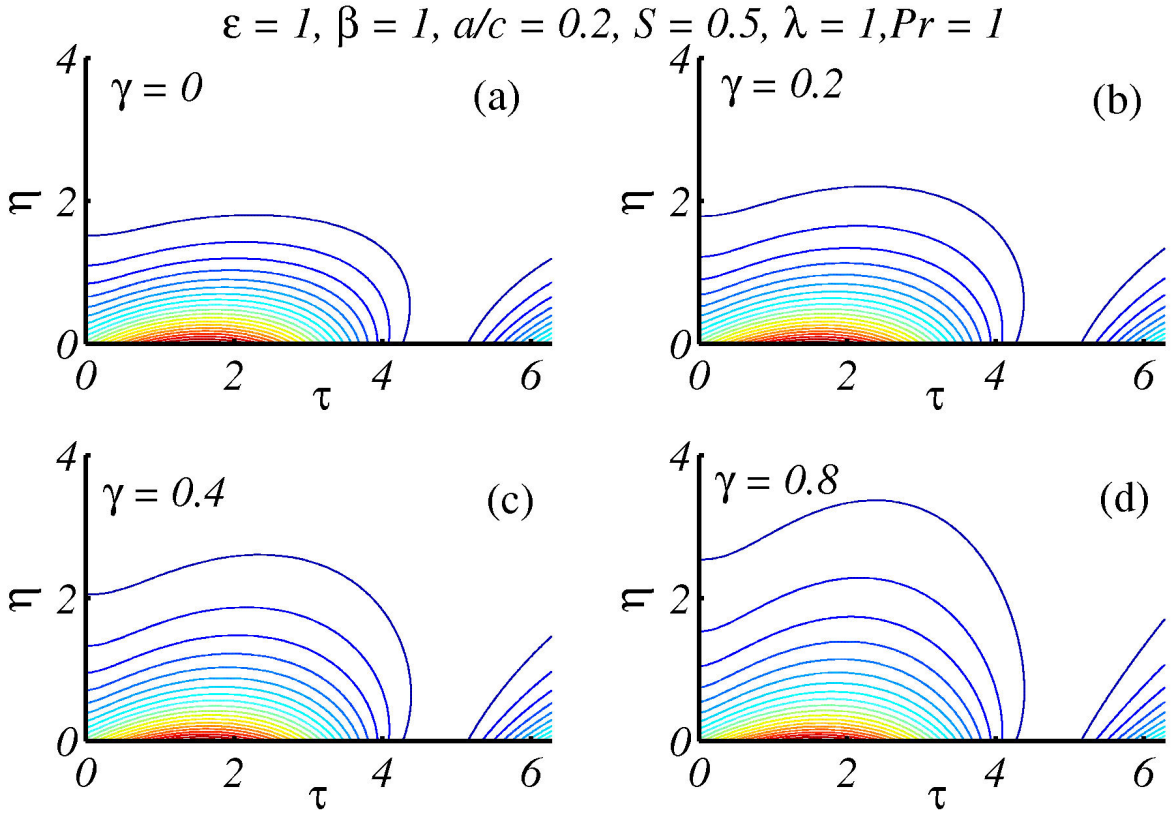

FIGURE 14. Isotherms for different values of curvature parameter γ.

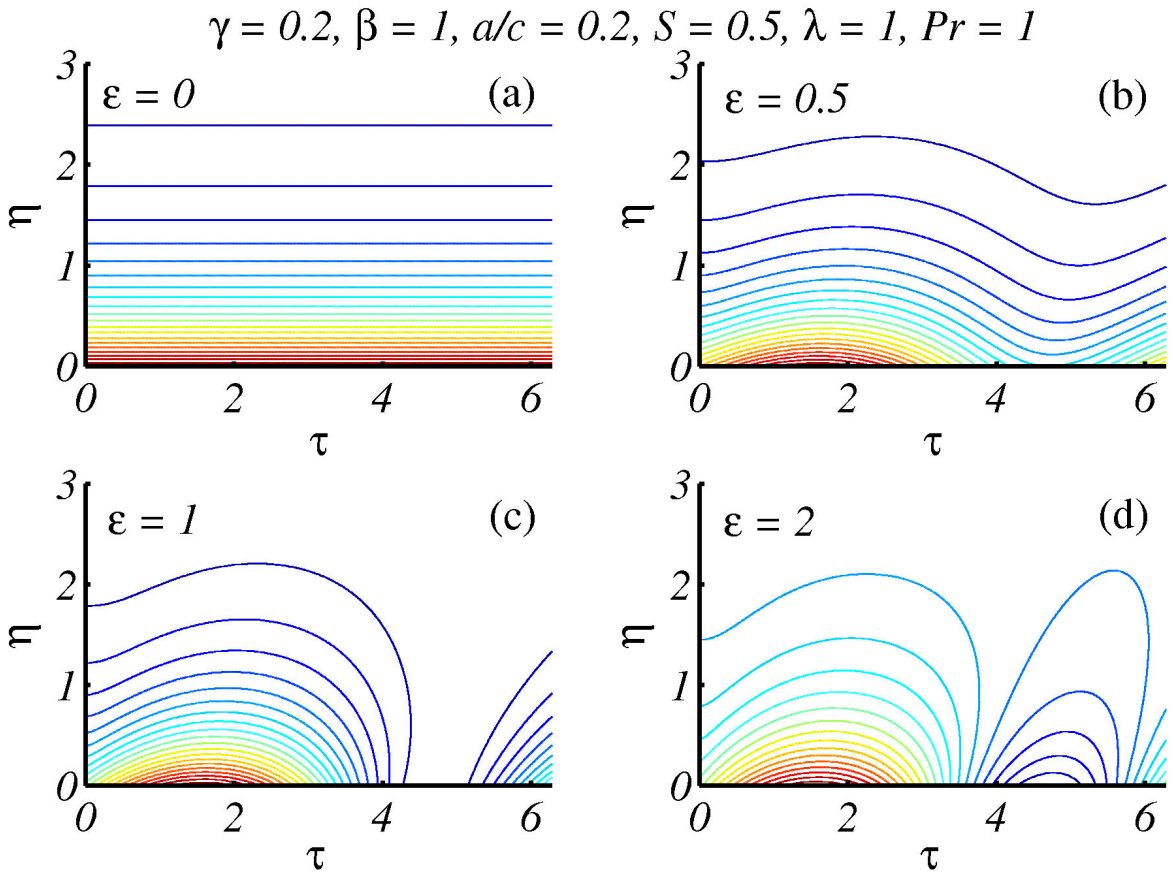

FIGURE 15. Isotherms for different values of amplitude of temperature oscillations ϵ.

ues of skin friction and Nusselt number against (τ) for different values of (ϵ). It is noted that amplitude of oscillations in the values of skin friction and Nusselt number increases with increase in (ϵ). It is also perceived that as the values of (ϵ) drop, the amplitude of oscillations in skin friction and Nusselt number also diminish for ($\epsilon = 0$), the case of constant surface temperature is recovered. The effect of Prandtl number (Pr) on heat transfer rate is observed in Fig. 13. The heat transfer rate enhances due to increase in Prandtl number (Pr) and amplitude of oscillation become larger for large values of Prandtl number (Pr) against time (τ). Figures 14 and 15 demonstrate the isotherms for curvature parameter (γ) and amplitude of temperature oscillations (ϵ). Due to increase in curvature parameter (γ) and amplitude of temperature oscillations (ϵ), a pattern of increasing behavior in sinusoidal nature of isotherms is clearly visible. Table III is constructed to exhibit the behavior of sundry parameters on skin friction coefficient ($Re_z^{1/2}C_f$) and local Nusselt number ($Re_z^{-1/2}Nu_z$). It is important to mention that negative values of local Nusselt number represent that heat is transferred from surface of cylinder to the fluid.

5. Conclusion

In this paper, unsteady mixed convection stagnation point flow due to stretching cylinder with sinusoidal wall temperature is reported. The governing partial differential equations are transformed into dimensionless form. The obtained partial differential equations are solved by an efficient and accurate finite difference scheme known as Keller box method. It is noted that the assisting buoyant flow increases the velocity profile and opposing buoyant flow decreases the velocity profile. It is apparent that as the amplitude of temperature oscillation drop, the amplitude of oscillations in skin friction and Nusselt number also diminish. The heat transfer rate increases due to increase in Prandtl number and amplitude of oscillation also increases with passage of time. Most importantly, this phenomenon of maximizing heat transfer near the stagnation point flow over a stretching cylinder can be enhanced by introducing the sinusoidal heat at the surface of the cylinder.

TABLE III. Values of $Re_z^{1/2}C_f$ and $(Re_z^{-1/2}Nu_z)$ for various parameter a/c, γ, λ, ϵ, β, S and Pr.

Pr	γ	a/c	λ	β	ϵ	S	$Re_z^{1/2}C_f, (Re_z^{-1/2}Nu_z)$			
							$t=0$	$t=\pi/4$	$\pi/2$	$t=\pi$
0.7	0	0	1	1	1	0.5	-0.7657	-0.5798	-0.3786	-0.6515
	0.2			1			-0.8034	-0.5861	-0.411	-0.6803
							(1.1508)	(2.3036)	(2.4750)	(0.8097)
		0.2					-0.714	-0.4985	-0.328	-0.6007
							(1.1857)	(2.3446)	(2.5236)	(0.8530)
			0				-0.2075	-1.2075	-1.2075	-1.2075
							(1.1158)	(2.2353)	(2.3479)	(0.7137)
				1.5			-0.2075	-1.2075	-1.2075	-1.2075
							(1.1158)	(2.3632)	(2.418)	(0.5696)
					1.5		-0.2075	-1.2075	-1.2075	-1.2075
							(1.1158)	(2.987)	(3.0691)	(0.2965)
1.0			-1				-1.7312	-1.9999	-2.278	-2.1029
							(1.3039)	(3.529)	(3.5352)	(0.1079)
	0.4						-1.8222	-2.0928	-2.3769	-2.2172
							(1.3628)	(3.6805)	(3.7137)	(0.1349)
		1					-0.3432	-0.5936	-0.8064	-0.4937
							(1.7024)	(4.1352)	(4.3674)	(0.8606)
				2			-0.3432	-0.5706	-0.7776	-0.5163
							(1.7024)	(4.3265)	(4.4671)	(0.6346)
					2		-0.3432	-0.6465	-0.9241	-0.5777
							(1.7024)	(5.1987)	(5.3753)	(0.2686)
7			1.5			-0.5	0.353	0.6352	0.899	0.5762
							(1.977)	(7.683)	(6.9611)	(-1.4708)
	0.6						0.3526	0.6346	0.8982	0.5761
							(2.0626)	(7.8986)	(7.2232)	(-1.3965)
		1.2					0.6807	0.9606	1.2176	0.8896
							(2.1204)	(7.9825)	(7.3444)	(-1.2899)

Nomenclature

a, c	Dimensionless constant
R	Radius of cylinder
C_f	Skin friction coefficient
c_p	specific heat at constant pressure
f	Dimensionless stream function
k	Thermal conductivity of fluid
l	reference length
Nu_z	Nusselt number
p	Pressure
Pr	Prandtl number
c_p	specific heat at constant pressure
q_w	Surface heat flux
Re_z	Local Reynolds number
r	Radial coordinate
T	Fluid temperature
T_w	Temperature at the surface of cylinder
T_∞	Ambient fluid temperature
u	Radial velocity component
V_e	Free stream velocity
V_w	Stretching velocity of cylinder
v	Axial velocity component
z	Axial coordinate
	Greek symbols
β	Unsteady parameter
β_t	Thermal expansion coefficient
γ	Transverse curvature
ϵ	Amplitude of temperature oscillation
η	Similarity variable
θ	Dimensionless temperature
ν	Kinematic viscosity
μ	Dynamic viscosity

τ	Time
τ_w	Surface shear stress
ρ	Density
ψ	Stream function
	Subscripts
w	Conditions at the surface
∞	Conditions at infinity

1. G.I. Burde, *J. Fluids Eng.* **117** (1995) 189-191.
2. K. Heimenz, *Dinglers Polytechn J.* **326** (1911) 321-324.
3. F. Homann, *Z. Angew. Math. Mech.* **16** (1936) 153-164.
4. H. Schlichting, and K. Bussmann, *Luftfahrtforschung, Ser. B,* **7** (1943) 25.
5. E.R.G. Eckert, *VDI-Forschungsheft,* **416** (1942) 1-24.
6. P.D. Ariel, *J. Appl. Mech.* **61** (1994) 976-978.
7. T. Altan, S. Oh, and H. Gegel, *Metal Forming Fundamentals and Applications* American Society of Metals, (Metals Park, Michigan, USA, 1979).
8. E.G. Fisher, *Extrusion of Plastics* (Wiley, New York, USA, 1976).
9. T.C. Chiam, *J. Phys. Soc. Jpn.* **63** (1994) 2443-2455.
10. T. R. Mahapatra, and A.S. Gupta, *Acta Mechanica* **152** (2001) 191-196
11. T. R. Mahapatra, and A.S. Gupta, *Heat Mass Transfer* **38** (2002) 517-521.
12. R. Nazar, N. Amin, D. Filip, and I. Pop, *Int. J. Eng. Science* **42** (2004) 1241-1253.
13. M. Mustafaa, T. Hayat, I. Pop, S. Asghar, and S. Obaidat, *Int. J. Heat Mass Transfer* **54** (2011) 255588-5594.
14. K. Bhattacharyya, S. Mukhopadhyay, and G.C. Layek, *Int. J. Heat and Mass Transfer* **54** (2011) 308-313.
15. P.R. Sharma, and G. Singh, *Journal of Applied fluid mechanics* **2** (2009) 13-21.
16. K. Bhattacharyya, and K. Vajravelu, *Commun. Nonlinear Sci. Num. Simulation,* **17** (2012) 2728-2734.
17. T. Javed, A. Ghaffari, and H. Ahmad, *Canadian Journal of Physics* **93** (2015) 1138-1143.
18. C.Y. Wang, *Physics of Fluids* **31** (1988) 466-468.
19. A. Ishak, R. Nazar, and Ioan Pop, *Convers Manage* **49** (2008) 3265-3269.
20. A. Ishak, R. Nazar, and Ioan Pop, *Applied Mathematical Modelling,* **32** (2008) 2059-2066.
21. S. Mukhopadhyay, *Journal of Petroleum Science and Engineering* **96** (2012) 73-78.
22. Z. Abbas, A. Majeed, and T. Javed, *Heat Transfer Research* **44** (2013) 703-718.
23. N. Bachok, and A. Ishak, *Malaysian J. Mathematical Sci.,* **4** (2010) 159-169.
24. H. R. Ashorynejad, H. R. Ashorynejad, M. Sheikholeslami, I. Pop, and D.D. Ganji, *Heat and Mass Transfer,* **49** (2013) 427-436.
25. T. Javed, I. Mustafa, *Asia-Pacific J. Chem. Eng.* **10** (2015) 184-192.
26. A. Majeed, T. Javed, A. Ghaffari, and M. M. Rashidi, *Alexandria Engineering Journal* **54** (2015) 1029-1036.
27. T. Javed, A. Majeed, and I. Mustafa, *Rev. Mex. Fis.* **61** (2015) 450-457.
28. J. H. Merkin and I. Pop, *Int. J. Heat and Mass Transfer* **43** (2000) 611-621.
29. A. Ishak, R. Nazar, and I. Pop, *Meccanica* **44** (2009) 369-375.
30. T. Cebeci and P. Bradshaw, *Physical and Computational Aspects of Convective Heat Transfer,* Springer New York (1984).